Molecular Therapy
Nucleic Acids
Original Article

AAV-Anti-miR-214 Prevents Collapse of the Femoral Head in Osteonecrosis by Regulating Osteoblast and Osteoclast Activities

Cheng Wang,[1,3,5] Weijia Sun,[2,5] Shukuan Ling,[2] Yu Wang,[1] Xin Wang,[1] Haoye Meng,[1] Yuheng Li,[2,4] Xueling Yuan,[1] Jianwei Li,[2] Ruoxi Liu,[1] Dingsheng Zhao,[2] Qiang Lu,[1] Aiyuan Wang,[1] Quanyi Guo,[1] Shibi Lu,[1] Hua Tian,[3] Yingxian Li,[2] and Jiang Peng[1]

[1]Institute of Orthopedics, Peking Key Lab of Regenerative Medicine in Orthopaedics, Key Lab of Chinese PLA, Chinese PLA General Hospital, Beijing, China; [2]State Key Laboratory of Space Medicine Fundamentals and Application, China Astronaut Research and Training Center, Beijing, China; [3]Department of Orthopedics, Peking University Third Hospital, Beijing, People's Republic of China; [4]The Key Laboratory of Aerospace Medicine, Ministry of Education, The Fourth Military Medical University, Xi'an, Shanxi, China

Osteonecrosis of the femoral head, an intractable but common disease that eventually triggers collapse of the femoral head, is characterized by increased osteoclast activity and markedly decreased osteoblast activity in the necrotic region of the femoral head. MicroRNA (miRNA)-214 (miR-214) may play important roles in vertebrate skeletal development by inhibiting osteoblast function by targeting activating transcription factor 4 (ATF4) and promoting osteoclast function via phosphatase and tensin homolog (PTEN). This study revealed significantly increased levels of miR-214 in necrotic regions, with commensurate changes in the numbers of its target cells (both osteoblasts and osteoclasts). To investigate whether targeting miR-214 could prevent femoral head collapse, we constructed an adeno-associated virus (AAV)-associated anti-miR-214 (AAV-anti-miR-214) and evaluated its function *in vivo*. AAV-anti-miR-214 promoted osteoblast activity and diminished osteoclast activity, effectively preventing collapse of the femoral head in a rat model of osteonecrosis.

INTRODUCTION

Osteonecrosis of the femoral head (ONFH) is a progressive refractory disease[1] resulting from various causes, including long-term high-dose glucocorticoids, intemperance, connective tissue diseases, and several forms of hematosis.[2,3] Our previous study using clinical samples of human femoral heads with osteonecrosis revealed that the necrotic regions showed significant variations in bone microstructure, with low bone mineral density and less trabecular bone than normal, as well as microfractures and small regions of bone resorption. In addition, the necrotic regions showed higher osteoclast activity and lower osteoblast activity.[4] Thus, we hypothesized that collapse of the femoral head involves changes in the activities of osteoblasts and osteoclasts, which gradually increases the number of bone resorption regions, enlarging their overall area during the progression of ONFH. Therefore, we investigated whether changes in the activities of osteoblasts and osteoclasts in the early stages of ONFH could prevent collapse of the femoral head.

MicroRNAs (miRNAs) are small 20- to 22-nt noncoding RNAs that play significant roles in the post-transcriptional regulation of various cellular processes.[5–8] Recently, miRNAs have gained heightened attention owing to their important roles in regulating the pathological progression of several diseases.[9–12] In bones, miRNAs regulate many processes including differentiation of osteoblasts and osteoclasts, orchestration of bone programming, and management of cell fate.[13–16] Bone remodeling is a continuous process requiring the physiological coupling of osteoclast and osteoblast activities.[17,18] miR-214 is highly conserved in vertebrates and is encoded within a larger noncoding RNA, the Dnm3 opposite strand. In previous work, we showed that miR-214 directly targets activating transcription factor 4 (ATF4) to inhibit osteoblast activity, thus preventing bone formation.[19] In addition, miR-214 affected phosphatidylinositol 3-kinase (PI3K)/Akt pathway activity by targeting phosphatase and tensin homolog (PTEN), downregulating PTEN levels, increasing osteoclast activity, and reducing bone mineral density.[20]. Therefore, the double regulatory actions of miR-214 suggest that this RNA may potentially serve as a valuable therapeutic target in certain bone diseases, particularly those involving changes in osteoblast and osteoclast activities.

An adeno-associated virus (AAV) is a small RNA virus[21–23] that can serve as a valuable carrier of therapeutic RNAs, as it infects a wide

Received 25 January 2019; accepted 15 September 2019;
https://doi.org/10.1016/j.omtn.2019.09.030.

[5]These authors contributed equally to this work.

Correspondence: Jiang Peng, Institute of Orthopedics, Peking Key Lab of Regenerative Medicine in Orthopaedics, Key Lab of Chinese PLA, Chinese PLA General Hospital, 28 Fuxing Road, Beijing 100853, People's Republic of China.
E-mail: pengjiang301@126.com
Correspondence: Yingxian Li, State Key Laboratory of Space Medicine Fundamentals and Application, China Astronaut Research and Training Center, No. 26 Beiqing Road, Haidian District, Beijing 100094, China.
E-mail: yingxianli@aliyun.com
Correspondence: Hua Tian, Department of Orthopedics, Peking University Third Hospital, 49 Huayuan North Road, Beijing 100191, People's Republic of China.
E-mail: tianhua@bjmu.edu.cn

This is an open access article under the CC BY-NC-ND license (http://creativecommons.org/licenses/by-nc-nd/4.0/).

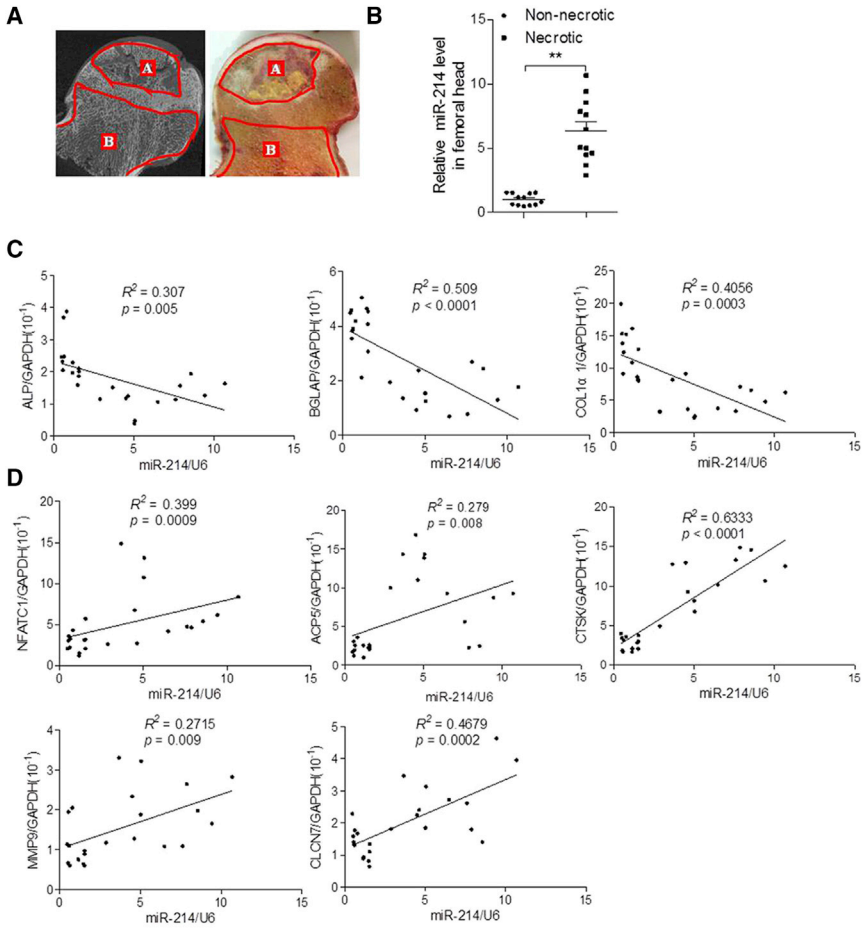

Figure 1. miR-214 Expression Correlates with Osteonecrosis of the Femoral Head

(A) Representative images of the femoral head. A, necrotic area; B, healthy (non-necrotic) area. (B) miR-214 levels were determined by RT-PCR and quantitative real-time PCR in necrotic and non-necrotic areas of human femoral heads with osteonecrosis. miR-214 levels were normalized to *U6*. Necrotic area group, n = 12; non-necrotic area group, n = 12. (C) Correlation analyses between mRNA levels of miR-214 and alkaline phosphatase (ALP), osteocalcin (BGLAP), collagen1 α1 (COL1α1) in bone specimens from patients with ONFH. miR-214 levels were normalized to U6. mRNA levels were normalized to GAPDH. For each group, n = 12. All data are presented as mean ± SEM. **p < 0.01. (D) Correlation analyses between mRNA levels of miR-214 and nuclear factor of activated T cells 1 (NFATc1), acid phosphatase 5 (ACP5), tartrate-resistant, cathepsin K (CTSK), matrix metallopeptidase 9 (MMP9), and chloride voltage-gated channel 7 (CLCN7) in bone specimens from patients with ONFH. miR-214 levels were normalized to U6. mRNA levels were normalized to GAPDH. Each group, n = 12. All data are presented as mean ± standard error of the mean (SEM) **P < 0.01.

range of hosts, has a long expression time, and wields low immunogenicity.[24–26] Recently, the European Medicines Agency approved the first gene therapy using AAV as the carrier of a drug aimed at curing lipoprotein lipase deficiency. Increasingly, researchers have focused on the use of AAV as a carrier of genetic materials in an effort to cure diseases.[27–29]

In the present study, we revealed upregulated miR-214 expression in femoral heads from patients with ONFH. In these samples, osteoclast activity was increased and osteoblast activity was decreased. We designed an AAV construct that expressed GFP and anti-miR-214 (AAV-anti-miR-214). We found that AAV-anti-miR-214 promoted osteoblast activity and inhibited osteoclast activity *in vivo* in rat femoral heads injected with AAV-anti-miR-214. These results suggest that miR-214 may be a useful therapeutic target for preventing ONFH.

RESULTS

Correlation of miR-214 Expression with Osteoclast and Osteoblast Activity in the Necrotic Regions of Femoral Heads from Patients with ONFH

Femoral heads exhibiting osteonecrosis were collected from patients who underwent total hip replacement. Each femoral head was divided into necrotic and healthy regions based on micro-computed tomography (CT) imaging (Figure 1A), and samples from these two regions were analyzed via RT-PCR and quantitative real-time PCR. The results showed increased miR-214 expression in the necrotic regions compared to healthy regions (Figure 1B). Expression of miR-214 was negatively correlated with expression of the bone formation marker genes alkaline phosphatase (*ALP*), osteocalcin (*BGLAP*), and collagen1 α1 (*COL1α1*), and positively correlated with expression of the osteoclastogenesis marker genes nuclear factor of activated T cells 1 (*NFATc1*), acid phosphatase 5 (*ACP5*), tartrate-resistant, cathepsin K (*CTSK*), matrix metallopeptidase 9 (*MMP9*), and chloride voltage-gated channel 7 (*CLCN7*) in bone specimens from patients with ONFH (Figures 1C and 1D).

AAV-Anti-miR-214 Promotes Osteoblast Function and Inhibits Osteoclast Function *In Vitro*

To determine the feasibility of the use of miR-214 as a therapeutic target for preventing ONFH, we constructed an AAV that expressed GFP and AAV-anti-miR-214. To investigate the effect of AAV-anti-miR-214 *in vitro*, we incubated AAV-anti-miR-214 with mouse osteoblasts and osteoclasts; simultaneously, we incubated anti-miR-214 with osteoblasts and osteoclasts as a positive control. Fluorescent signal was detected in osteoblasts and osteoclasts following treatment with AAV-anti-miR-214 or AAV-normalized control (NC) (Figures 2A and 2B). The intracellular miR-214 level was substantially downregulated following treatment with anti-miR-214 or AAV-anti-miR-214 (Figures 2C and 2G). In contrast, we observed upregulated mRNA levels of the osteoblast marker genes *Alp*, *Bglap*, and *Col1α1* (Figure 2D). Consistent with the changes in *ALP*

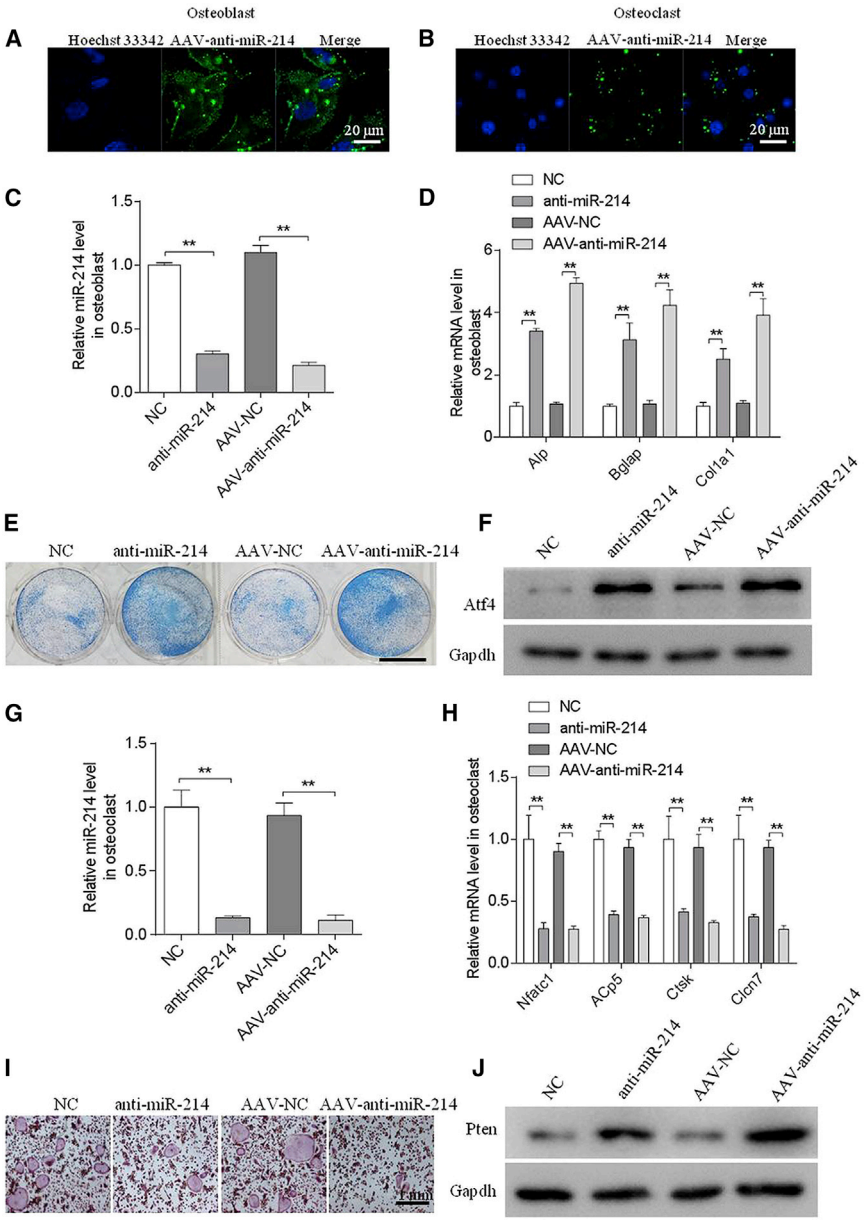

Figure 2. Adeno-Associated Virus-Anti-miR-214 Increased Osteogenic Activity and Decreased Osteoclastic Activity *In Vitro*

(A and B) Representative images of GFP in mouse primary osteoblasts (A) and osteoclasts (B) incubated with AAV-anti-miR-214 or AAV-normalized control (NC). (C) RT-PCR and quantitative real-time PCR analyses of miR-214 levels in mouse primary osteoblasts following incubation with anti-miR-214, NC, AAV-anti-miR-214, or AAV-NC for 2 days. (D) RT-PCR and quantitative real-time PCR analyses of *ALP*, *Bglap*, and *Col1α1* mRNA levels in mouse primary osteoblasts following incubation with anti-miR-214, NC, AAV-anti-miR-214, or AAV-NC for 2 days. (E) Representative images of ALP staining of mouse primary osteoblasts following incubation with anti-miR-214, NC, AAV-anti-miR-214, or AAV-NC for 2 days. Scale bar, 7.8 mm. (F) Western blot analyses of ATF4 levels in primary osteoblasts following incubation with anti-miR-214, NC, AAV-anti-miR-214, or AAV-NC for 2 days. (G) RT-PCR and quantitative real-time PCR analyses of miR-214 levels in receptor activator of nuclear factor κB ligand (RANKL)-induced bone marrow-derived macrophages (BMMs) following incubation with AAV-anti-miR-214 or AAV-NC for 4 days. (H) RT-PCR and quantitative real-time PCR analyses of *Nfatc1*, *Acp5*, *Ctsk*, and *Clcn7* mRNA levels in RANKL-induced BMMs following incubation with AAV-anti-miR-214 or AAV-NC for 4 days. (I) Western blot analyses of PTEN protein levels in RANKL-induced BMMs following incubation with AAV-anti-miR-214 or AAV-NC for 4 days. (J) Representative images of tartrate-resistant acid phosphatase (TRAP) staining of RANKL-induced BMMs following incubation with AAV-anti-miRNA-214 or AAV-NC for 4 days. All data are presented as mean ± SEM from three independent experiments. $^{**}p < 0.01$.

mRNA levels, cells with lower miR-214 levels showed enhanced ALP staining (Figure 2E). miR-214 inhibits osteoblast function by targeting ATF4; concordantly, we detected significantly greater amounts of ATF4 protein in the anti-miR-214 and AAV-anti-miR-214 treatment groups than in the NC and AAV-NC groups (Figure 2F). In addition, the osteoclasts marker genes *Nfatc1*, *Acp5*, *Ctsk*, and *Clcn7* showed downregulated mRNA expression levels (Figure 2H). Functionally, the numbers of TRAP-positive, multinucleated osteoclasts were markedly reduced in the anti-miR-214 or AAV-anti-miR-214 treatment groups compared to the negative control group (Figure 2I). miR-214 promotes osteoclast function by targeting PTEN; accordingly, the PTEN protein level was increased in the anti-miR-214 or AAV-anti-miR-214 treatment groups (Figure 2J).

Evaluation of the Efficiency of AAV-Anti-miR-214 *In Vivo*

To investigate the effectiveness of AAV infection *in vivo*, we established ONFH in rats and injected the heads with AAV-anti-miR-214 (model + AAV-anti-miR-214) or AAV-NC (model + NC) using an in-house pressurizing injector. We tracked GFP expression in live rats using a whole-animal fluorescent imaging system at 2, 4, 6, and 8 weeks postsurgery (Figure 3A). No fluorescence was detected in the test or control rats at any time point. The model + AAV-anti-miR-214 and model + NC groups showed strong signals in the right hips up to 8 weeks postinjection (Figure 3B).

To further confirm the expression of AAV-anti-miR-214 in the rat femoral head, we assessed GFP signals in frozen sections of right femoral head samples collected at 2 and 8 weeks postsurgery. Green fluorescence was detected in the model + AAV-anti-miR-214 and

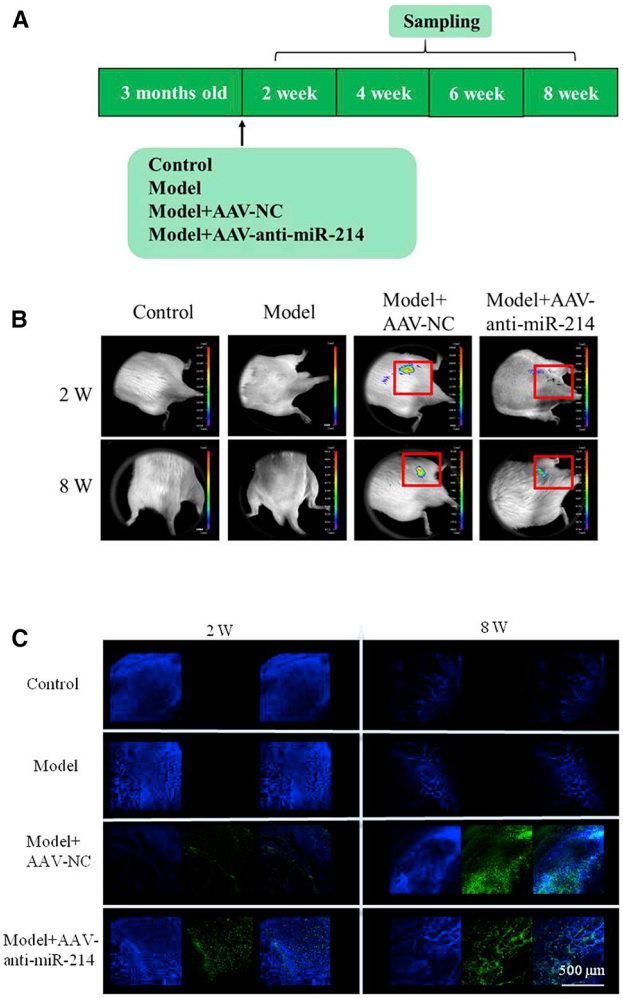

Figure 3. GFP and miR-214 Expression *In Vivo*

(A) Schematic diagram illustrating the experimental design. Model, osteonecrosis of the femoral head in rat. (B) Live animal fluorescence imaging was used to monitor GFP expression at 2 and 8 weeks postsurgery. (C) Laser confocal microscopy was used to monitor GFP expression in frozen sections of rat femoral heads in the four groups at 2 and 8 weeks postsurgery. Scale bar, 500 μm. For each group, n = 6. All data are presented as mean ± SEM.

model + NC groups, but not in the model and control groups (Figure 3C).

AAV-Anti-miR-214 Promotes Bone Formation in a Model of Femoral Head Osteonecrosis

To assess the activity of AAV-anti-miR-214 *in vivo*, we measured miR-214 expression in the femoral heads of rats and found that expression of miR-214 was higher in bone of the model and model + NC groups compared to that in the control group at 2 and 8 weeks postsurgery. The miR-214 expression level in the model + AAV-anti-miR-214 groups was decreased to almost that of the control group (Figure 4A).

Bone histomorphometric analyses showed that the control group had a spherical femoral head with even thickness of the femoral neck, and the trabecular bone was structurally continuous and uniform in distribution. The model and model + NC groups showed a gradual collapse of the femoral head, with emergence of increasing numbers of bone resorption regions. In addition, the femoral neck became more slender, and some trabecular bone fractures developed with continuous loss of bone structure. In contrast, the model + AAV-anti-miR-214 groups showed no collapse or obvious bone resorption, and no deterioration in the appearance of the femoral head or neck, appearing similar to the control group.

Micro-CT revealed that the ratio of bone/tissue volume and bone mineral density were significantly higher in the model + AAV-anti-miR-214 group than in the model and model + NC groups at 2 and 8 weeks postinjection of AAV-anti-miR-214 (Figures 4B–4D). H&E staining of the model and model + NC groups showed a gradual increase in the number of empty lacunae, decreased trabecular bone, and development of greater numbers of trabecular bone fractures. In contrast, the model + AAV-anti-miR-214 group showed trabecular bone, bone cell density, and number of lacunae that were similar to those of the control group (Figure 4E).

AAV-Anti-miR-214 Treatment Increases Osteoblast Activity and Decreases Osteoclast Activity in the Necrotic Regions of the Femoral Head

To investigate whether AAV-anti-miR-214 can regulate osteoblast and osteoclast activities, we measured expression levels of the osteoblast markers *ALP*, *Bgalp*, and *Col1α1* and the osteoclast markers *Acp5*, *Ctsk*, *Mmp9*, and *Clcn7* in rat bone. *ALP*, *Bgalp*, and *Col1α1* mRNA levels were significantly increased in the model + AAV-anti-miR-214 group compared to those in the model and model + NC groups (Figure 5A). *Acp5*, *Ctsk*, *Mmp9*, and *Clcn7* mRNA levels were significantly lower in the model + AAV-anti-miR-214 group than in the model and model + NC groups (Figure 5B). In functional terms, serum concentrations of ALP and OCN protein were substantially higher in the model + AAV-anti-miR-214 than in the model and model + NC groups (Figure 5C), while the concentrations of N-telopeptide of type I collagen (NTX-1) and C-telopeptide of type I collagen (CTX-1) were substantially lower (Figure 5D). These data suggest that *in vivo* treatment with AAV-anti-miR-214 promotes osteoblast activity and inhibits osteoclast activity in necrotic regions of the femoral head.

miR-214 promotes osteoclast function via the PTEN/PI3K/AKT pathway and inhibits osteoblast function by targeting ATF4. In our study, we found increased expression of miR-214 in the femoral head in the ONFH-induced model. Whereas PTEN protein levels were decreased in the model and model + NC groups, such levels were increased in the model + AAV-anti-miR-214 group. The p-Akt and Nfatc1 protein levels were higher in the model and model + NC groups than in the model + AAV-anti-miR-214 group. Osteoclast function was promoted and osteoblast function was inhibited in the model and model + NC groups. The ATF4 protein level was decreased

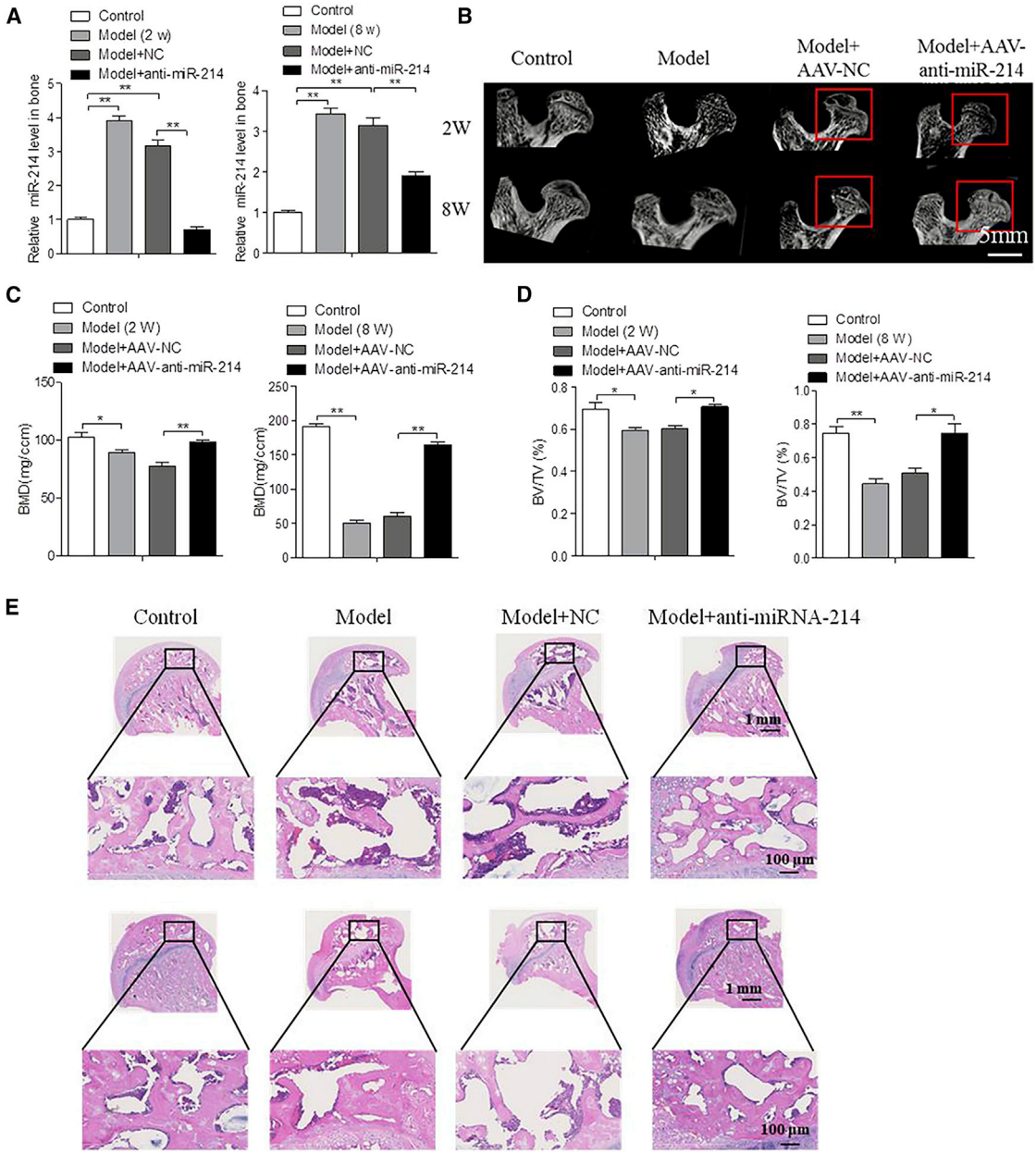

Figure 4. AAV-anti-RNA-214 Impedes Collapse of the Femoral Head in Osteonecrosis

(A) RT-PCR and quantitative real-time PCR analyses of miR-214 levels in the femoral head of rats among the groups at 2 and 8 weeks postsurgery. For each group, n = 6. (B) Representative three-dimensional images of the femoral head in the control, model, model + AAV-NC, and model + AAV-anti-miR-214 groups at 2 and 8 weeks postsurgery. Scale bar, 5 mm. For each group, n = 6. (C) Micro-computed tomography (CT) measurements of bone mineral density of the femoral heads from the control, model, model + AAV-NC, and model + AAV-anti-miR-214 groups at 2 and 8 weeks postsurgery. For each group, n = 6. (D) Micro-CT measurements of the ratio of trabecular bone volume to tissue volume of the femoral heads from the control, model, model + AAV-NC, and model + AAV-anti-miR-214 groups at 2 and 8 weeks postsurgery. For each group, n = 6. (E) H&E staining of rat femoral heads using paraffin sections from control, model, model + AAV-NC, and model + AAV-anti-miR-214 at 2 and 8 weeks postsurgery. Scale bar, 1 mm; for figures in black boxes, the scale bar represents 100 μm. All data are presented as mean ± SEM. *$p < 0.05$, **$p < 0.01$.

in the model and model + NC groups, but increased in the model + AAV-anti-miR-214 group (Figure 5E). Osteoblast function was inhibited; AAV-anti-miR-214 effectively regulated the functioning of osteoclasts and osteoblasts. The femoral heads of rats with osteonecrosis showed decreased levels of PTEN protein but increased levels of p-AKT and NFATC1 in the necrotic regions compared to healthy regions. The necrotic regions showed decreased ATF4 protein levels (Figure 5F). These results suggest that miR-214 promotes osteoclast

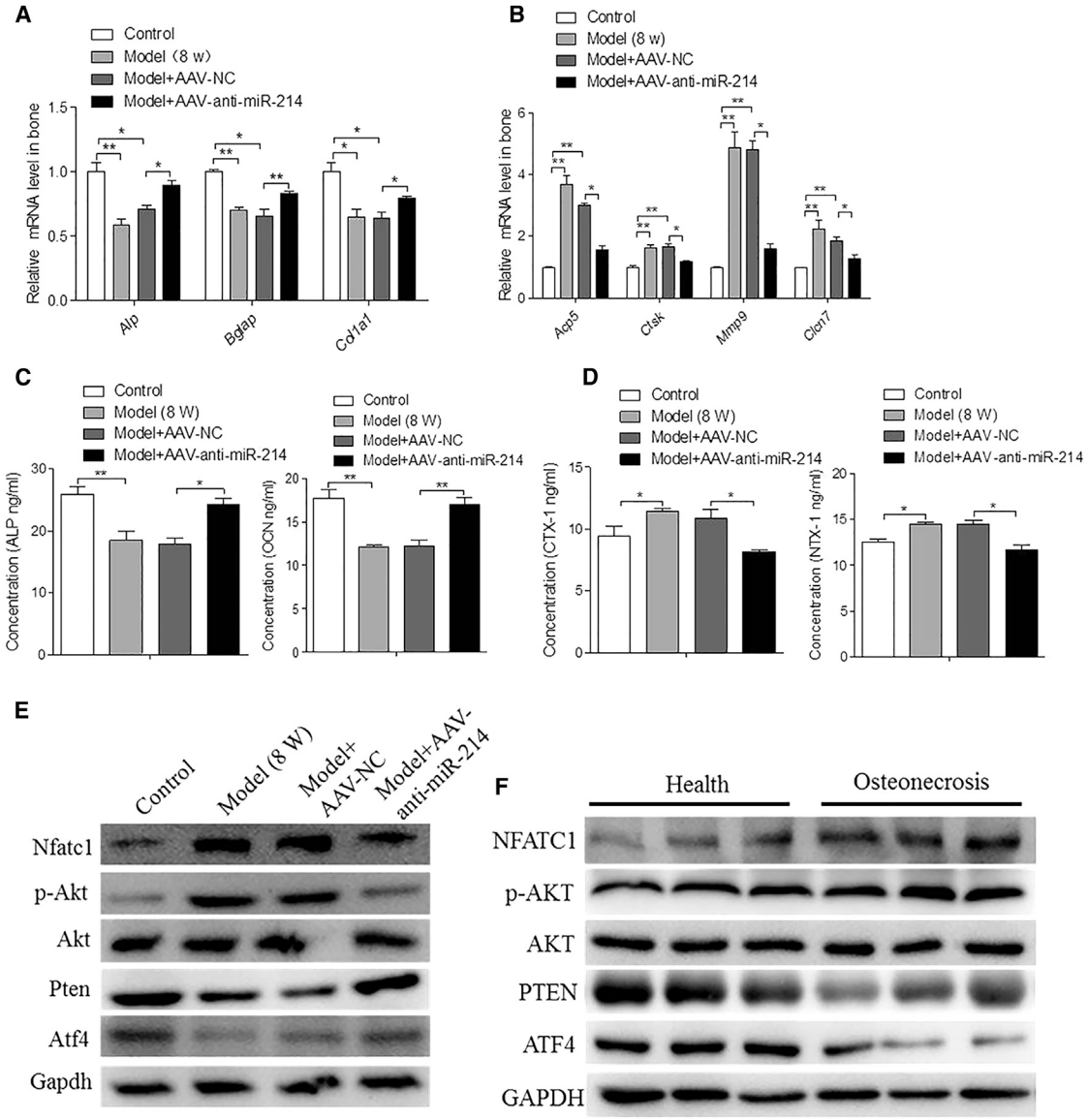

Figure 5. Inhibitory Role of AAV-Anti-miR-214 on Osteoclastic Activity and the Promotion of AAV-Anti-miR-214 on Osteogenic Activity

(a) RT-PCR and quantitative real-time PCR analyses of *ALP*, *Bglap*, and *Col1α1* mRNA levels in the femoral heads of rats among the various groups at 8 weeks postsurgery. For each group, n = 6. (B) RT-PCR and quantitative real-time PCR analyses of *Acp5*, *Ctsk*, *Mmp9*, and *Clcn7* mRNA levels in the femoral heads of rats from control, model, model + NC, and model + AAV-anti-miR-214 groups at 8 weeks postsurgery. For each group, n = 6. (C) ELISA analyses of ALP and OCN levels in rat serum from control, model, model + AAV-NC, and model + AAV-anti-miR-214 groups at 8 weeks postsurgery. For each group, n = 6. (D) ELISA analyses of CTX-1 and NTX-1 levels in rat serum from control, model, model + AAV-NC, and model + AAV-anti-miR-214 groups at 8 weeks post-surgery. For each group, n = 6. (E) Western blot analyses of Nfatc1, p-Akt, PTEN, and ATF4 protein levels in the femoral heads of rats in the various groups at 8 weeks postsurgery. GAPDH was used as the internal control. (F) Western blot analyses of NFATC1, p-AKT, PTEN, and ATF4 protein levels in the femoral heads of patients with osteonecrosis. GAPDH was used as the internal control. All data are presented as mean ± SEM from three independent experiments.

function via the PTEN/PI3K/AKT pathway and inhibits osteoblast function by targeting ATF4 when ONFH is in play.

DISCUSSION

This study showed that miR-214 expression was significantly elevated in the necrotic regions of human femoral heads exhibiting osteonecrosis. In addition, AAV-anti-mi-214 promoted osteoblast function and inhibited osteoclast function both *in vitro* and *in vivo* in rats. These results suggest that therapeutic inhibition of miR-214 during the early stages of femoral head degeneration in the ONFH rat model promotes bone formation, inhibits bone resorption, prevents femoral head collapse, and even reverses ONFH via an anabolic effect.

Collapse of the femoral head is a dynamic process with the progression of osteonecrosis. During bone repair and reconstruction, the numbers and activity levels of osteoblasts and osteoclasts also undergo great changes.[4] The entire process features repair and destruction, summed up by the phrase, "There's no making without breaking." Generally speaking, new bone formation features a series of processes, including osteoblast proliferation and differentiation, osteoid formation, and bone mineralization. However, osteoclast activity increases over a short period of time, significantly affecting the strength of the bony trabeculae. Therefore, the mechanical strength of the femoral head is inevitably reduced during repair and the head will collapse if it remains under long-term mechanical loading.[30]

Ideally, ONFH should be treated early. Before femoral head collapse, many therapeutic methods are available, including but not limited to high-pressure oxygen,[31] extracorporeal shock wave therapy,[32] core decompression,[33] and tantalum rod implantation.[34] However, no single method has shown complete success in preventing collapse. In addition, although total hip replacement relieves symptoms effectively, it is not the best option for young patients. Thus, the development of a more effective treatment preventing femoral head collapse is imperative.

Recently, the potential for using miRNA to treat ONFH has attracted increasing attention.[35] Yamasaki et al.[36] found that the expression levels of mature (primary) miR-210, VEGF, matrix metalloproteinase (MMP)-2, and MMP-7 were significantly higher in osteonecrotic femoral head samples than in osteoarthritic samples. Section-based *in situ* hybridization to detect mature miR-210 revealed that this material was expressed around necrotic areas, showing that miR-210 may play a role in ONFH pathogenesis. Wang et al.[37] used the Affymetrix GeneChip to identify miRNAs of bone marrow mesenchymal stem cells in a rat model of steroid-induced ONFH. They found that many miRNAs regulated osteogenic differentiation and that a decrease in miRNA-196a-5p might be important in the context of steroid-induced ONFH. Wang et al.[37] reported abnormally expressed miRNAs in the sera of patients with ONFH, suggesting their use as diagnostic markers. Zhao et al.[38] found that miRNA-34a alleviated the inhibitory effects of Dex on mesenchymal stem cells and osteoblasts, while facilitating Dex-mediated inhibitory effects on endothelial cells. These results suggested that miRNA-34a is an important regulator of both osteogenesis and angiogenesis, and might be a useful therapeutic target in patients with glucocorticoid-induced ONFH.[39] Zhao et al.[38] found that miR-145 targeted the osteoprotegrin (OPG)/ receptor activator of nuclear factor κB (RANK)/RANK ligand (RANKL signaling pathway and played a role in the development of steroid-induced necrosis of the femoral head. Hao et al.[40] investigated the role of miR-708 function in a steroid-induced ONFH model and found that inhibition of miR-708 rescued the suppressive effects of glucocorticoid on osteonecrosis. Glucocorticoid caused miR-708 overexpression in mesenchymal stem cells, suggesting that targeting miR-708 might be therapeutically useful for preventing and treating ONFH.

miR-214 is expressed widely in various tissues and cells, targeting a variety of genes involved in cancer development, the immune system, differentiation of skeletal muscle cells, protection of the heart from ischemic injury, and inhibition of angiogenesis.[41–44] Recently, it has received heightened interest, as it may function as both a diagnostic marker and therapeutic target for bone disease. Our results showed that miR-214 regulates the functions of both osteoblasts and osteoclasts. It directly targeted ATF4 to inhibit osteoblast activity and functioned via PTEN/PI3K/Akt to promote osteoclast function.

We found that miR-214 showed a significantly higher expression in the necrotic regions of human femoral heads with osteonecrosis and *in sera* from patients with ONFH than in other tissues/fluids. Consistently, osteoclast activity was promoted and osteoblast activity was inhibited in necrotic regions, indicating that miR-214 may mediate femoral head collapse in ONFH. This study employed the novel innovation of using anti-miR-214 to prevent such collapse. We constructed an AAV containing anti-miR-214 and assessed its function *in vivo* and *in vitro*. The virus replicated to produce sufficient amounts of anti-miR-214. AAV-anti-miR-214 promoted osteoblast function and inhibited osteoclast function. During osteonecrosis, AAV-anti-miR-214 regulated bone formation and bone resorption in two ways, postponing ONFH progression, and thus preventing the collapse of the femoral head associated with osteonecrosis.

Conclusion

This study suggests that AAV-anti-miR-214 has tremendous potential as a treatment for ONFH, and anti-miR-214 could be a valuable therapeutic agent for patients in the early stages of ONFH.

MATERIALS AND METHODS

Human Bone Preparation

Ten femoral heads with osteonecrosis were collected from patients undergoing total hip replacement. The patients were 45–65 years of age and were diagnosed via MRI. The classification of patients with and without ONFH was based on X-ray and MRI evaluation. The age distributions of the two groups were similar. All clinical procedures were approved by the Committee of Clinical Ethics of the General Hospital of the Chinese People's Liberation Army, Beijing, China.

Cell Culture

Mouse bone marrow cells were isolated from the femur and tibia of 2-month-old mice. Briefly, bone marrow cells were flushed and collected with α-minimal essential media (MEM). Cells were then cultured with complete α-MEM medium (α-MEM, 10% fetal bovine serum [FBS], and penicillin/streptomycin) in the presence of macrophage colony stimulating factor (M-CSF; 10 ng/mL, R&D Systems) for 1 day. Suspension cells were collected for osteoclast generation. Cells were cultured in complete medium with 30 ng/mL M-CSF and 50 ng/mL receptor activator of nuclear factor κB ligand (R&D Systems) for 4 days. The culture medium was replaced every 2 days.

Primary osteoblasts were isolated from the calvarial bone of newborn (1- to 3-day-old) mice by enzymatic digestion in α-MEM with 0.1%

collagenase and 0.2% dispase, and cultured in α-MEM with 10% FBS. After 2 days, cells were reseeded and cultured in osteogenic medium for the osteoblast differentiation assay. Osteogenic medium was prepared by supplementing the maintenance medium with 10 nM dexamethasone (Dex; Sigma-Aldrich), 50 μg/mL ascorbic acid (Sigma-Aldrich), and 10 mM β-glycerophosphate (Sigma-Aldrich).

Tartrate-Resistant Acid Phosphatase (TRAP) Staining

TRAP staining was performed using an acid phosphatase kit according to the manufacturer's instructions (Sigma-Aldrich, catalog no. 387). After 5 days of culture, RANKL-induced cells were fixed by immersion in fixative solution for 30 s at room temperature and rinsed thoroughly in deionized water. The plates were incubated in TRAP staining solution at 37°C for 1 h in the dark. Following removal of the TRAP solution, the plates were washed three times with distilled water. TRAP-positive multinuclear cells were counted under an inverted microscope (Nikon).

ALP Staining

ALP staining was monitored using a Vector Blue Substrate kit according to the manufacturer's instructions (Vector Laboratories, catalog no. SK-5300). The cells were fixed by immersion in a citrate-buffered acetone solution for 30 s, rinsed in deionized water for 45 s, then placed in ALP stain for 20–30 min. All procedures were performed in the dark.

RT-PCR and Quantitative Real-Time PCR

Total RNA was extracted from bone tissues or cells using TRIzol reagent (Invitrogen) according to the manufacturer's instructions. Cell samples were washed with PBS prior to TRIzol treatment. RNA (0.5 μg) was reverse transcribed using the PrimeScript RT reagent kit (Takara) according to the manufacturer's instructions. Stem-loop RT-PCR was used to quantify miR-214; 2 μL of cDNA was used to evaluate mRNA and miRNA expression by RT-PCR and quantitative real-time PCR using a SYBR Premix Ex TaqII kit (Takara). *GADPH* served as the NC for mRNA, and *RNU6* was used as the NC for miRNA measurements. Table 1 lists the primers used in this study.

AAV-Anti-miR-214 Production and Evaluation

AAV-anti-miR-214 was produced using an rno-miR-214-3P sponge in AAV-293 cells in combination with the expression of GFP (Hanheng, China). The right femoral heads of rats were examined using the Kodak In-Vivo Imaging System FX (Japan) to track GFP at 2 and 8 weeks postsurgery. We sacrificed the rats and harvested the femoral heads prior to generating frozen sections. After staining with DAPI for 5 min, we assessed the effects of AAV-anti-miR-214 via confocal microscopy (Olympus, Japan) at 2 and 8 weeks postsurgery.

ONFHs from Rats

The rats were divided into the following four groups: control (no procedure), model (ONFH model only), model + NC (ONFH model with injection of AAV into the right side of the femoral head), and model + AAV-anti-miR-214 (ONFH model with injection of AAV-anti-miR-214 into the right side of the femoral head). We used a traumatic method to establish the ONFH model. After exposing the femoral heads, we removed the round ligament, peeled the periosteum, and injected AAV (30 μL) or AAV-anti-miR-214 (30 μL) using an in-house pressurized injector. We closed each incision by layer and disinfected the wounds. Rats were sacrificed after 2 and 8 weeks.

Micro-CT

High-resolution micro-CT was used to evaluate the femoral heads *in vitro* using a 27-μm resolution instrument (GE Healthcare, USA) at 2 and 8 weeks post-surgery. Bone histomorphometric features were analyzed using GE MicroView software. Three regions ($0.5 \times 0.5 \times 0.5$ cm^3) were selected from the volumes of interest (beyond the line of the epiphysis). We calculated the ratio of trabecular bone volume to tissue volume and bone mineral densities.

Histological Evaluation

Femoral heads were harvested at 2 and 8 weeks postinjury (n = 4 per group), fixed for 3 days in 4% (v/v) paraformaldehyde, decalcified in 10% (w/v) EDTA for 4 weeks, embedded in paraffin, and cut into 7-μm sections. Panoramic scanning was performed after H&E staining.

Western Blot Analysis

Cells were lysed in lysis buffer (50 mM Tris [pH 7.5], 250 mM NaCl, 0.1% [w/v] SDS, 2 mM DTT, 0.5% [v/v] Nonidet P-40, 1 mM PMSF, and a protease inhibitor cocktail) on ice for 30 min. Protein fractions were collected by centrifugation at 12,000 × *g* at 4°C for 30 min, subjected to SDS-PAGE, and transferred to polyvinylidene difluoride membranes. The membranes were blocked with 5% (w/v) BSA and incubated with specific antibodies overnight. A horseradish-peroxidase-labeled secondary antibody was added, and bands were visualized using an Enhanced Chemiluminescence Kit (Pierce). The antibodies used were anti-Nfatc1, anti-p-Akt, anti-Akt, anti-PTEN, anti-ATF4, and anti-GADPH (all obtained from Cell Signaling Technology).

ELISA

To measure the serum levels of ALP, osteocalcin (OCN), NTX-1, and CTX-1, sera samples were collected and stored at −80°C prior to the assay. ELISAs of ALP, OCN, CTX-1, and NTX-1 featured conventional colorimetric detection using kits according to the manufacturer's instructions (Cloud-Clone). Briefly, 50 μL of sera was pipetted in duplicate into the wells of precoated ELISA plates. Then, 50 μL of standard or sample was added to each well, followed by 50 μL of detection reagent A. All samples were immediately mixed by shaking, incubated for 1 h at 37°C, aspirated, and washed three times. Next, 100 μL of detection reagent B was added, followed by incubation for 30 min at 37°C, aspiration, and five washes. Finally, 90 μL of substrate solution was added, followed by incubation for 10–20 min at 37°C; 50 μL of stop solution was added, and absorptions at 450 nm were read immediately.

Table 1. mRNA Primers

	Mouse Primers
Gapdh-forward	5′-AACATCAAATGGGGTGAGGCC-3′
Gapdh-reverse	5′-GTTGTCATGGATGACCTTGGC-3′
Alp-forward	5′-ATCTTTGGTCTGGCTCCCATG-3′
Alp-reverse	5′-TTTCCCGTTCACCGTCCAC-3′
Bglap-forward	5′-CCAAGCAGGAGGGCAATA-3′
Bglap-reverse	5′-TCGTCACAAGCAGGGTCA-3′
Col1α1-forward	5′-GGGACCAGGAGGACCAGGAAGT-3′
Col1α1-reverse	5′-GGAGGGCGAGTGCTGTGCTTT-3′
Acp5-forward	5′-GCGACCATTGTTAGCCACATACG-3′
Acp5-reverse	5′-CGTTGATGTCGCACAGAGGGAT-3′
Nfatc1-forward	5′- ACGCTACAGCTGTTCATTGG-3′
Nfatc1-reverse	5′- CTTTGGTGTTGGACAGGATG-3′
Ctsk-forward	5′-CAGCAGAGGTGTGTACTATG-3′
Ctsk-reverse	5′-GCGTTGTTCTTATTCCGAGC-3′
Clcn-forward	5′-ACACAGCGTCTAATCACAAC-3′
Clcn-reverse	5′-GTCCTTCAGCCTCAGTCG-3′
	Human Primers
GAPDH-forward	5′-ACAACTTTGGTATCGTGGAAGG-3′
GAPDH-reverse	5′-GCCATCACGCCACAGTTTC-3′
ALP-forward	5′-GTGAACCGCAACTGGTACTC-3′
ALP-reverse	5′-GAGCTGCGTAGCGATGTCC-3′
BGLAP-forward	5′-GGCGCTACCTGTATCAATGG-3′
BGLAP-reverse	5′-GTGGTCAGCCAACTCGTCA-3′
COL1A1-forward	5′-GAGGGCCAAGACGAAGACATC-3′
COL1A1-reverse	5′-CAGATCACGTCATCGCACAAC-3′
NFATc1-forward	5′-AAGAGGAAGTACAGCCTCAACG-3′
NFATc1-reverse	5′-TCTCCTTTCCGAAGTTCAAIGT-3′
CTSK-forward	5′-AAGCCAGACAACAGATTTCCAT-3′
CTSK-reverse	5′-GGATCATTTGAAGCACAAACAA-3′
ACP5-forward	5′-GGAGGGAATAAAGGCTCAGG-3′
ACP5- reverse	5′-GGAACTCAGCAAAGGTGAGC-3′
MMP9-forward	5′-CGTCGGTCCGTCCGCTA-3′
MMP9-reverse	5′-TCAGCCCTCACCTCGGTACT-3′
CLCN7- forward	5′-CGTGAGGATCCCAATGAGGG-3′
CLCN7- reverse	5′-CCTTCATAATCCCGGGGCCT-3′
	Rat Primers
Gapdh-forward	5′-TCACCACCATGGAGAAGGC-3′
Gapdh-reverse	5′-GCTAAGCAGTTGGTGGTGCA-3′
Alp-forward	5′-GGGAAGATGTGGCGGTCTTT-3′
Alp-reverse	5′-TAGTTCTGCTCATGGACGCC-3′
Bglap-forward	5′-CCCGTGTTGGTTAATGCCAC-3′
Bglap-reverse	5′-GTCCGCTAGCTCGTCACAAT-3′
Col1α1-forward	5′-CCCAGCGGTGGTTATGACTT-3′
Col1α1-reverse	5′-AACGGCCACCATCTTGAGAC-3′
Acp5-forward	5′-AGTCAAATCCGCCCCTTCTTT-3′
Acp5-reverse	5′-TCGGTCTCCCGGTCTTTTAG-3′
MMP9-forward	5′-CTACAGCTTTGCTGCCCCTC-3′
MMP9-reverse	5′-TGGAGGTTTTCAGGTCTCGG-3′
Ctsk-forward	5′-CCTTAGTCTACCATTACAGTAGCCA-3′
Ctsk-reverse	5′-CTGCTGTTGAGAATCTGTTGTCT-3′
Clcn7-forward	5′-TCTAAGAAAGTGTCTTGGTCCGGC-3′
Clcn7-reverse	5′-GTCTCCTCGTCAGGTTGCCC-3′

Statistical Analyses

All numerical data are expressed as mean ± SEM from at least three independent samples. Student's t test was used for statistical evaluations of two group comparisons. Statistical analyses with more than two groups were performed using one-way ANOVA. All statistical analyses were performed with Prism software (GraphPad Prism for Windows, version 6.0). $p < 0.05$ was considered to indicate statistical significance.

AUTHOR CONTRIBUTIONS

J.P. , Y.L. and H.T. conceived the study. S.L. and S.L. designed experiments. C.W. and W.S. designed and performed the majority of the experiments, analyzed data and prepared the manuscript. H.M., X.Y., R.L.,Q.L., Y.L., Y.W., J.L. and D.Z. performed experiments; A.W., Q.G. analyzed and critically discussed the data. All authors discussed the results and implications and commented on the manuscript at all stages.

CONFLICTS OF INTEREST

The authors declare no competing interests.

ACKNOWLEDGMENTS

This work was supported in part by grants from the National Natural Science Foundation of China (81572148, 81972047, 81603008, 31630038, 91740114, 31800994, and 31700741) to J.P., Yingxian Li, W.S., and Yuheng Li, and State Key Lab of Space Medicine Fundamentals and Application Grant (SMFA15B03) to Yuheng Li.

REFERENCES

1. Sakamoto, Y., Yamamoto, T., Sugano, N., Takahashi, D., Watanabe, T., Atsumi, T., Nakamura, J., Hasegawa, Y., Akashi, K., Narita, I., et al.; Japanese Research Committee on Idiopathic Osteonecrosis of the Femoral Head (2017). Genome-wide association study of idiopathic osteonecrosis of the femoral head. Sci. Rep. *7*, 15035.

2. Amanatullah, D.F., Strauss, E.J., and Di Cesare, P.E. (2011). Current management options for osteonecrosis of the femoral head: part 1, diagnosis and nonoperative management. Am. J. Orthop. *40*, E186–E192.

3. Amanatullah, D.F., Strauss, E.J., and Di Cesare, P.E. (2011). Current management options for osteonecrosis of the femoral head: part II, operative management. Am. J. Orthop. *40*, E216–E225.

4. Wang, C., Wang, X., Xu, X.L., Yuan, X.L., Gou, W.L., Wang, A.Y., Guo, Q.Y., Peng, J., and Lu, S.B. (2014). Bone microstructure and regional distribution of osteoblast and osteoclast activity in the osteonecrotic femoral head. PLoS ONE *9*, e96361.

5. Rigoutsos, I., and Furnari, F. (2010). Gene-expression forum: decoy for microRNAs. Nature *465*, 1016–1017.
6. Chitwood, D.H., and Timmermans, M.C. (2010). Small RNAs are on the move. Nature *467*, 415–419.
7. Ambros, V. (2004). The functions of animal microRNAs. Nature *431*, 350–355.
8. Kosik, K.S. (2010). MicroRNAs and cellular phenotypy. Cell *143*, 21–26.
9. Persson, H., Søkilde, R., Häkkinen, J., Pirona, A.C., Vallon-Christersson, J., Kvist, A., Mertens, F., Borg, Å., Mitelman, F., Höglund, M., and Rovira, C. (2017). Frequent miRNA-convergent fusion gene events in breast cancer. Nat. Commun. *8*, 788.
10. Browne, G., Taipaleenmäki, H., Stein, G.S., Stein, J.L., and Lian, J.B. (2014). MicroRNAs in the control of metastatic bone disease. Trends Endocrinol. Metab. *25*, 320–327.
11. Xue, M., Liu, H., Zhang, L., Chang, H., Liu, Y., Du, S., Yang, Y., and Wang, P. (2017). Computational identification of mutually exclusive transcriptional drivers dysregulating metastatic microRNAs in prostate cancer. Nat. Commun. *8*, 14917.
12. Gao, B., and Zheng, L. (2013). microRNA Expression in rat apical periodontitis bone lesion. Bone Res. *1*, 170–185.
13. Eskildsen, T., Taipaleenmäki, H., Stenvang, J., Abdallah, B.M., Ditzel, N., Nossent, A.Y., Bak, M., Kauppinen, S., and Kassem, M. (2011). MicroRNA-138 regulates osteogenic differentiation of human stromal (mesenchymal) stem cells in vivo. Proc. Natl. Acad. Sci. USA *108*, 6139–6144.
14. Itoh, T., Nozawa, Y., and Akao, Y. (2009). MicroRNA-141 and -200a are involved in bone morphogenetic protein-2-induced mouse pre-osteoblast differentiation by targeting distal-less homeobox 5. J. Biol. Chem. *284*, 19272–19279.
15. Huang, J., Zhao, L., Xing, L., and Chen, D. (2010). MicroRNA-204 regulates Runx2 protein expression and mesenchymal progenitor cell differentiation. Stem Cells *28*, 357–364.
16. Kuang, W., Zheng, L., Xu, X., Lin, Y., Lin, J., Wu, J., and Tan, J. (2017). Dysregulation of the miR-146a-Smad4 axis impairs osteogenesis of bone mesenchymal stem cells under inflammation. Bone Res. *5*, 17037.
17. Alliston, T., and Derynck, R. (2002). Medicine: interfering with bone remodelling. Nature *416*, 686–687.
18. Marx, J. (2004). Coming to grips with bone loss. Science *305*, 1420–1422.
19. Wang, X., Guo, B., Li, Q., Peng, J., Yang, Z., Wang, A., Li, D., Hou, Z., Lv, K., Kan, G., et al. (2013). miR-214 targets *ATF4* to inhibit bone formation. Nat. Med. *19*, 93–100.
20. Zhao, C., Sun, W., Zhang, P., Ling, S., Li, Y., Zhao, D., Peng, J., Wang, A., Li, Q., Song, J., et al. (2015). miR-214 promotes osteoclastogenesis by targeting Pten/PI3k/Akt pathway. RNA Biol. *12*, 343–353.
21. Aschauer, D.F., Kreuz, S., and Rumpel, S. (2013). Analysis of transduction efficiency, tropism and axonal transport of AAV serotypes 1, 2, 5, 6, 8 and 9 in the mouse brain. PLoS ONE *8*, e76310.
22. Yu, W., Mookherjee, S., Chaitankar, V., Hiriyanna, S., Kim, J.W., Brooks, M., Ataeijannati, Y., Sun, X., Dong, L., Li, T., et al. (2017). *Nrl* knockdown by AAV-delivered CRISPR/Cas9 prevents retinal degeneration in mice. Nat. Commun. *8*, 14716.
23. Ruozi, G., Bortolotti, F., Falcione, A., Dal Ferro, M., Ukovich, L., Macedo, A., Zentilin, L., Filigheddu, N., Gortan Cappellari, G., Baldini, G., et al. (2015). AAV-mediated in vivo functional selection of tissue-protective factors against ischaemia. Nat. Commun. *6*, 7388.
24. Bevan, A.K., Duque, S., Foust, K.D., Morales, P.R., Braun, L., Schmelzer, L., Chan, C.M., McCrate, M., Chicoine, L.G., Coley, B.D., et al. (2011). Systemic gene delivery in large species for targeting spinal cord, brain, and peripheral tissues for pediatric disorders. Mol. Ther. *19*, 1971–1980.
25. Shen, X., Storm, T., and Kay, M.A. (2007). Characterization of the relationship of AAV capsid domain swapping to liver transduction efficiency. Mol. Ther. *15*, 1955–1962.
26. Prasad, K.M., Xu, Y., Yang, Z., Acton, S.T., and French, B.A. (2011). Robust cardiomyocyte-specific gene expression following systemic injection of AAV: in vivo gene delivery follows a Poisson distribution. Gene Ther. *18*, 43–52.
27. Yang, S., Hao, L., McConnell, M., Zhou, X., Wang, M., Zhang, Y., Mountz, J.D., Reddy, M., Eleazer, P.D., Li, Y.P., and Chen, W. (2013). Inhibition of Rgs10 expression prevents immune cell infiltration in bacteria-induced inflammatory lesions and osteoclast-mediated bone destruction. Bone Res. *1*, 267–281.
28. Kemaladewi, D.U., Maino, E., Hyatt, E., Hou, H., Ding, M., Place, K.M., Zhu, X., Bassi, P., Baghestani, Z., Deshwar, A.G., et al. (2017). Correction of a splicing defect in a mouse model of congenital muscular dystrophy type 1A using a homology-directed-repair-independent mechanism. Nat. Med. *23*, 984–989.
29. Bennett, J., Wellman, J., Marshall, K.A., McCague, S., Ashtari, M., DiStefano-Pappas, J., Elci, O.U., Chung, D.C., Sun, J., Wright, J.F., et al. (2016). Safety and durability of effect of contralateral-eye administration of AAV2 gene therapy in patients with childhood-onset blindness caused by *RPE65* mutations: a follow-on phase 1 trial. Lancet *388*, 661–672.
30. Fan, M., Peng, J., Wang, A., Zhang, L., Liu, B., Ren, Z., Xu, W., Sun, J., Xu, L., Xiao, D., et al. (2011). Emu model of full-range femoral head osteonecrosis induced focally by an alternating freezing and heating insult. J. Int. Med. Res. *39*, 187–198.
31. Uzun, G., Mutluoglu, M., Ersen, O., and Yildiz, S. (2016). Hyperbaric oxygen therapy in the treatment of osteonecrosis of the femoral head: a review of the current literature. Undersea Hyperb. Med. *43*, 189–199.
32. Alves, E.M., Angrisani, A.T., and Santiago, M.B. (2009). The use of extracorporeal shock waves in the treatment of osteonecrosis of the femoral head: a systematic review. Clin. Rheumatol. *28*, 1247–1251.
33. Villa, J.C., Husain, S., van der List, J.P., Gianakos, A., and Lane, J.M. (2016). Treatment of pre-collapse stages of osteonecrosis of the femoral head: a systematic review of randomized control trials. HSS J. *12*, 261–271.
34. Pakos, E.E., Megas, P., Paschos, N.K., Syggelos, S.A., Kouzelis, A., Georgiadis, G., and Xenakis, T.A. (2015). Modified porous tantalum rod technique for the treatment of femoral head osteonecrosis. World J. Orthop. *6*, 829–837.
35. Li, Z., Yang, B., Weng, X., Tse, G., Chan, M.T.V., and Wu, W.K.K. (2018). Emerging roles of MicroRNAs in osteonecrosis of the femoral head. Cell Prolif. *51*, e12405.
36. Yamasaki, K., Nakasa, T., Miyaki, S., Yamasaki, T., Yasunaga, Y., and Ochi, M. (2012). Angiogenic microRNA-210 is present in cells surrounding osteonecrosis. J. Orthop. Res. *30*, 1263–1270.
37. Wang, B., Yu, P., Li, T., Bian, Y., and Weng, X. (2015). MicroRNA expression in bone marrow mesenchymal stem cells from mice with steroid-induced osteonecrosis of the femoral head. Mol. Med. Rep. *12*, 7447–7454.
38. Zhao, J.J., Wu, Z.F., Wang, L., Feng, D.H., and Cheng, L. (2016). MicroRNA-145 mediates steroid-induced necrosis of the femoral head by targeting the OPG/RANK/RANKL signaling pathway. PLoS ONE *11*, e0159805.
39. Peng, W.X., Ye, C., Dong, W.T., Yang, L.L., Wang, C.Q., Wei, Z.A., Wu, J.H., Li, Q., Deng, J., and Zhang, J. (2017). MicroRNA-34a alleviates steroid-induced avascular necrosis of femoral head by targeting *Tgif2* through OPG/RANK/RANKL signaling pathway. Exp. Biol. Med. (Maywood) *242*, 1234–1243.
40. Hao, C., Yang, S., Xu, W., Shen, J.K., Ye, S., Liu, X., Dong, Z., Xiao, B., and Feng, Y. (2016). miR-708 promotes steroid-induced osteonecrosis of femoral head, suppresses osteogenic differentiation by targeting SMAD3. Sci. Rep. *6*, 22599.
41. Huang, P.S., Lin, Y.H., Chi, H.C., Chen, P.Y., Huang, Y.H., Yeh, C.T., Wang, C.S., and Lin, K.H. (2017). Thyroid hormone inhibits growth of hepatoma cells through induction of miR-214. Sci. Rep. *7*, 14868.
42. Hsieh, T., Liu, Y., Chang, T., Liang, M., Chen, H., Wang, H., Yen, Y., and Wong, T.T. (2018). Global DNA methylation analysis reveals miR-214-3p contributes to cisplatin resistance in pediatric intracranial nongerminomatous malignant germ cell tumors. Neuro-oncol. *20*, 519–530.
43. Xu, C., He, T., Li, Z., Liu, H., and Ding, B. (2017). Regulation of HOXA11-AS/miR-214-3p/EZH2 axis on the growth, migration and invasion of glioma cells. Biomed. Pharmacother. *95*, 1504–1513.
44. Jan, M.I., Khan, R.A., Ali, T., Bilal, M., Bo, L., Sajid, A., Malik, A., Urehman, N., Waseem, N., Nawab, J., et al. (2017). Interplay of mitochondria apoptosis regulatory factors and microRNAs in valvular heart disease. Arch. Biochem. Biophys. *633*, 50–57.